Baseline Refinement for Topographic Phase Estimation using External DEM

Chang Won Lee, Wooil M. Moon

ESI[3] Laboratory, School of Earth and Environmental Sciences (SEES), Seoul National University, Seoul, 151-742, Korea (bosscq@eos1.snu.ac.kr, wmoon@eos1.snu.ac.kr)

Abstract: Multitemporal interferometric SAR has became an useful geodetic tool for monitoring Earth's surface deformation, generation of precise DEM, and land cover classification even though there still exist certain constraints such as temporal and spatial decorrelation effects, atmospheric artifacts and inaccurate orbit information. The Korea where nearly all areas are heavily vegetated, JERS-1 SAR has advantages in monitoring surface deformations and environmental changes in that it uses 4-times longer wavelength than ERS-1/2 or RADARSAT SAR system.

For generating differential SAR interferogram and differential coherence image for deformation mapping and temporal change detection, respectively, topographic phase removal process is required utilizing a reference interferogram or external DEM simulation. Because the SAR antenna baseline parameter for JERS-1 is less accurate than those of ERS-1/2, one can not estimate topographic phases from an external DEM and the residual phase appears in differential interferogram.

In this paper, we examined topographic phase retrieval method utilizing an external DEM. The baseline refinement is carried out by minimizing the differences between the measured unwrapped phase and the reference points of the DEM.

1. Introduction

Multitemporal SAR interferometry has became an useful geodetic tool for generation of high precision DEM and monitoring Earth surface changes such as earthquake deformation, sea ice movement, volcano inflation and land subsidence [1]. In addition coherence imagery can be used for random surface change detection and environmental process monitoring [4,6]. In Korea where most regions except urban areas are heavily vegetated and highly humid, the JERS-1 L-band SAR system has definite advantages over the C-band system in that it is less sensitive to temporal decorrelation caused by various surface changes. For detecting ground deformation from measured SAR phase information or unbiased coherence estimation, topographic phase must be removed. The 2-pass method utilizes external DEM instead of an interferogram for topographic phase removal. One of the merits of the 2-pass methods is that the DEM coregistered to the radar coordinate can be regarded as many GCPs and that manual human intervention can be minimized.

Inaccurate baseline parameters calculated from JERS-1 orbit ephemeris result in residual fringe patterns in differential interferograms. In the case of ERS-1/2 which uses more accurate orbit information than JERS-1 or RADARSAT, baseline refinement is required.

Baseline refinement is carried out in two steps. First, a simulated interferogram is generated from the DEM using an initial baseline parameter. Second, the relation between the measured unwrapped phase of the interferogram and the reference phase computed from the DEM is used for correcting baseline after building baseline model.

2. Methodology

Interferogram simulation method

For the generation of topographic phase from a reference DEM, the input DEM must be resampled and registered to the master radar coordinate. Using the following relation between the radar geometry and DEM,

the DEM height is assigned to each output pixel.

$$\hat{l} \cdot \hat{V} = 0 \text{ where, } \hat{l} = \frac{\vec{P}(t) - \vec{P}_{DEM}}{|\vec{P}(t) - \vec{P}_{DEM}|} \quad \hat{V} = \frac{\vec{V}(t)}{|\vec{V}(t)|} \tag{1}$$

where $\hat{l}$: unit look vector, $\hat{V}$: unit platform velocity vector, $\vec{P}(t)$: platform position vector, $\vec{P}_{DEM}$: DEM position vector, $\vec{V}(t)$: platform velocity vector.

But the initial orbit is not known precisely, a simulated SAR image using simulated radar intensity, is first generated.

$$I = \frac{\cos^2 \theta_i}{\sqrt{1 - \cos^2 \theta_i}} \tag{2}$$

where $\cos\theta_i = -\hat{l} \cdot \hat{n}$, θ_i: local incidence angle and $\hat{n}$: surface outward unit normal vector

Using the offset parameters derived from the amplitude correlation between simulated SAR and actual amplitude SAR image, fine registration is done.

After synthesizing the interferogram from registered DEM, the simulated interferometric phase is subtracted from the interferogram to remove the topographic fringes. Differential interferogram devoid of topographic phases has smooth residual fringe rate. To improve both measurement accuracy and phase unwrapping, multilooking of range and azimuth pixel size and adaptive phase noise filtering method is carried out.

Baseline modeling

Baseline is defined as the difference between two antennas when a specific target is imaged and a function of time and target position.

$$\vec{b} \equiv \vec{P}_2 - \vec{P}_1 = \rho_1 \hat{l}_1 - \rho_2 \hat{l}_2 \tag{3}$$

where $\vec{b}$: interferometric baseline, $\vec{P}_i$: antenna i position vector, ρ_i: antenna i range to target and $\hat{l}_i$: unit look vector from antenna i to the target.

Figure 1 shows the SAR imaging geometry in the *sch* coordinate system where *s* is an along-track coordinate, *c* is an across-track coordinate, and *h* is the height above a sphere.

The unit vector $\hat{l}_i^{sch_i}$ from the antenna i to the target in *sch* coordinates may be expressed as [1]:

$$\hat{l}_i^{sch_i} = \begin{bmatrix} \cos\theta_i \sin\gamma_i \cos\beta + \sin\theta_i \sin\beta \\ -\cos\theta_i \sin\gamma_i \sin\beta + \sin\theta_i \cos\beta \\ -\cos\theta_i \cos\gamma_i \end{bmatrix} \tag{4}$$

where θ_i: look angle of the antenna i, γ_i : pitch angle of antenna i, β : squint angle, and a left-looking geometry has been assumed.

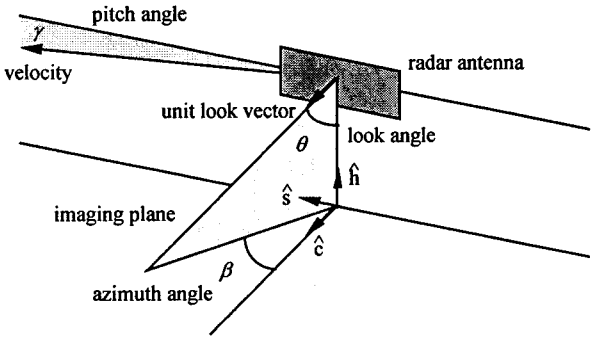

Fig. 1. SAR imaging geometry in *sch* coordinate

If one assume the pitch angle of antenna 1 is zero, then the unit look vector, $\hat{l}_1$ and $\hat{l}_2$ can be expressed as follow in each *sch* coordinate as :

$$\hat{l}_1^{sch_1} = \begin{bmatrix} \sin\theta_1 \sin\beta \\ \sin\theta_1 \cos\beta \\ -\cos\theta_1 \end{bmatrix} \tag{6}$$

$$\hat{l}_2^{sch_2} = \begin{bmatrix} \cos\theta_2 \sin\gamma \cos\beta + \sin\theta_2 \sin\beta \\ -\cos\theta_2 \sin\gamma \sin\beta + \sin\theta_2 \cos\beta \\ -\cos\theta_2 \cos\gamma \end{bmatrix}. \tag{7}$$

The interferogram phase may have a component that varies with azimuth position and this implies that orbits converge or diverge slightly. Then one can define divergence angle η in the *sc*-plane from the antenna track 1 to the antenna track 2. Then the unit look vector in the *sch* coordinate at the antenna 2 can be transformed to *sch* coordinate at the antenna 1.

$$\hat{l}_2^{sch_1} = \begin{bmatrix} \cos\eta & -\sin\eta & 0 \\ \sin\eta & \cos\eta & 0 \\ 0 & 0 & 1 \end{bmatrix} \hat{l}_2^{sch_2} \tag{8}$$

$\tan\eta \approx \sin\eta$,

$\tan\gamma \approx \sin\gamma$,

$\cos\beta \approx 1$, and

$\cos(\beta-\eta) \approx 1$.

With the above assumptions for JERS-1 SAR antenna, the baseline can be expressed as

$$\vec{b} = \begin{bmatrix} b_s \\ b_c \\ b_h \end{bmatrix} = \begin{bmatrix} b_c \tan\beta + \rho_2 \sin\theta_2 \tan\eta - \rho_2 \cos\theta_2 \tan\gamma \\ \rho_1 \sin\theta_1 \cos\beta - \rho_2 \sin\theta_2 \cos\beta \cos\eta \\ -\rho_1 \cos\theta_1 + \rho_2 \cos\theta_2 \cos\gamma \end{bmatrix}. \tag{9}$$

By removing the target-dependent along track offset, one obtains the modified baseline model

$$\vec{b}' = \vec{b} - \begin{bmatrix} \Delta s_T \\ 0 \\ 0 \end{bmatrix} = \begin{bmatrix} 0 \\ b_c \\ b_h \end{bmatrix} = \begin{bmatrix} \Delta s_0 + (k s_2 - s_1) - \Delta s_T \\ b_{c0} + \dot{b}_c (s_1 + \Delta s_T) \\ b_{h0} + \dot{b}_h (s_1 + \Delta s_T) \end{bmatrix} \tag{10}$$

where Δs_T : target-dependent along-track offset, Δs_0 : along-track constant offset, k : along-track scale factor between the s_1 and s_2 coordinates, b_{c0} : initial cross-track baseline, b_{h0} : initial vertical baseline, $\dot{b}_c$: cross-track baseline rate of change, and $\dot{b}_h$: vertical baseline rate of change.

Introducing the along-track variable $s = s_1 + \Delta s_T$, this baseline model may be written concisely as

$$\vec{b}'(s) = \begin{bmatrix} \Delta s_0 + (k s_2 - s) \\ b_{c0} + \dot{b}_c s \\ b_{h0} + \dot{b}_h s \end{bmatrix}. \tag{11}$$

The measurements available for the baseline estimation are the range and azimuth offsets. The azimuth offset Δs_{offset} can be estimated from the registration process.

Using the equation $s_2 = s_1 + \Delta s_{offset}$, a relationship between the azimuth offset measurement Δs_{offset} and the model parameter Δs_0 can be written as

$$\Delta s_0 + k(s_1 + \Delta s_{offset}) - s_1 - \Delta s_T = 0. \tag{12}$$

The range offset $\Delta\rho_{offset}$ is from the unwrapped phase and reference range offset $\Delta\rho$ is estimated from the GCPs picked from the reference DEM.

$$\Delta\rho_{offset} = (\lambda / 4\pi)\varphi \tag{13}$$

$$\Delta\rho = \rho_1 \left(\sqrt{1 - 2(\hat{l}_1 \cdot \hat{b})\rho_1^{-1} + b^2 \rho_1^{-2}} - 1 \right) \tag{14}$$

where φ : unwrapped, unflattened interferometric phase.

$$\Delta\rho_0 = \Delta\rho - \Delta\rho_{offset} \tag{15}$$

$\Delta\rho_0$: range constant offset

The baseline parameter to be estimated are as follows.

$$X^T = \begin{bmatrix} b_{c0} & b_{h0} & \dot{b}_c & \dot{b}_h & k & \Delta s_0 & \Delta\rho_0 \end{bmatrix}. \tag{16}$$

The observation-state relationship may be written as

$$Y_i = G_i(X) + \varepsilon_i \quad \text{where} \quad Y_i = \begin{bmatrix} (\Delta\rho_{offset})_i \\ (\Delta s_{offset})_i \end{bmatrix}, \tag{17}$$

$$G_i(X) = \begin{bmatrix} \Delta\rho - \Delta\rho_0 \\ \frac{1}{k}(s_1 + \Delta s_T - \Delta s_0) - s_1 \end{bmatrix}, \quad i = 1, \ldots, l.$$

Here, Y_i is the observation vector, $G_i(X)$ is the measurement model, ε_i is the measurement noise and l is the number of offset measurements, and s_1 is determined from the along-track spacing and the line number of offset measurement i.

Because the number of observations is greater than the number of parameters to be estimated, a set of constraints must be developed to select one estimate from the many possible solutions. The approach used here was the minimization of the sum of the square of the observation erros $J(X^*)$

$$J(X^*) = \sum_{i=1}^{l} \varepsilon_i^{*T} \varepsilon_i^* = \sum_{i=1}^{l} \left[Y_i - G_i(X^*) \right]^T \left[Y_i - G_i(X^*) \right] \tag{18}$$

where X^* is initial guess.

This is a nonlinear least squares problem and this procedure is iterated until the difference between updated and previous parameter vectors is less than a given

threshold.

Topographic phase corrected coherence estimation

For surface change detection, isolation of only the effects of temporal decorrelation from other factors such as thermal noise, baseline, terrain slope, co-registration, and atmospheric condition is necessary.

Coherence of the complex radar signals $z_1 = |z_1|e^{i\varphi_1}$, $z_2 = |z_2|e^{i\varphi_2}$ can be estimated by sample coherence by averaging the two radar echoes of the neighboring pixels within an average window as

$$\gamma = \frac{\left|\sum_{j=1}^{n}|z_{1j}||z_{2j}|e^{i\varphi_{12}}\right|}{\sqrt{\sum_{j=1}^{n}|z_{1j}|^2}\sqrt{\sum_{j=1}^{n}|z_{2j}|^2}} \tag{19}$$

where $\varphi_{12} = \varphi_1 - \varphi_2$ and n is the number of averaging pixels. But this sample coherence is based on the assumption that the scene is locally homogenous and stationary. In a non-homogenous scene where topographic phase is dominant, these assumptions are not valid and topographic phase is the source of non-stationarity resulting in coherence bias [6].

Differential coherence uses as φ_{12} topographic phase corrected phase instead of flat earth corrected phase, which can be thought of additional product of DInSAR processing.

3. Results and Discussion

A JERS-1 SAR data pair used for baseline refinement was acquired on November 25, 1997 and Febrary 21, 1998 respectively. The resolution of DEM used for the interferogram simulation was one arc second and each height value was arranged by latitude and longitude coordinates.

Due to the inaccurate orbit state vectors provided in the leader file simulated SAR image using equation (1) (Fig. 2a,b) have large offset with real SAR amplitude image. Although the gross offset between the simulated SAR and the real SAR image indicates inaccuracy in the master orbit, for the generation of differential interferogram, only relative geometry estimation between master and slave orbit was performed.

Using the initial baseline parameters estimated from the orbit state vectors, a simulated interferogram was generated (Fig. 2d). Because more accurate initial baseline is, lower fringe frequency appears in the differential interferogram, baseline estimation through coregistration offset parameters may be an alternative for making later phase unwrapping process easier.

After adaptive interferogram filtering (proposed by [5]) was done to 4-look (range) by 20-look (azimuth) image to reduce phase noise, residual interferogram was unwrapped using branch-cut algorithm. Then simulated topography (the same one subtracted before the phase unwrapping) was restored to the unwrapped phase.

Quality of the unwrapped phase used for the estimation of baseline parameter can be evaluated by the phase standard deviation. In this work, only σ_φ less than 0.1 phase values were used.

Among the parameters to be estimated in (16), $k = 1$ and Δs_{offset} was assumed zero.

Using the unwrapped phase, four baseline parameters and the range offset was estimated as follows.

	b_{c0}	b_{h0}	$\dot{b}_c$	$\dot{b}_h$
initial	-409.67	-289.84	1.91xe-04	-3.26xe-05
refined	-452.32	-279.50	1.96xe-04	-3.41xe-05

4. Conclusion

In this study, 2-pass DInSAR processing method was performed on JERS-1 SAR data for effective topographic phase removal using external DEM. Inaccurate orbit state vectors provided in the header file caused residual fringe patterns in the differential interferogram. After building baseline model, baseline parameters were refined using a reference DEM. Accurate initial baseline

parameter can make phase unwrapping easier by reducing the fringe frequency.

Topographic phase calculated from DEM after baseline refinement can be used for unbiased coherence estimation.

This work is a preparatory research for application of differential interferometry to surface change detection of Kyungsang basin in southeast Korea.

Acknowledgment

This research is partially supported by BK21 program through the School of Earth and Environmental Sciences (SEES), Seoul National University, Korea.

References

[1] S.M., Buckley, 2000, Radar Interferometry Measurement of Land Subsidence. The University of Texas at Austin, PhD thesis. 3698 p.

[2] P.A. Rosen, S. Hensley, et al., 1996, Surface deformation and coherence measurements of Kilauea Volcano, Hawaii, from SIR-C radar interferometry. Journal of Geophysical Research, 101, 23109-23125.

[3] D.C. Ghiglia and M.D. Pritt, 1998, Two-dimensional Phase Unwrapping. John Wiley & Sons, 493 p.

[4] H.A., Zebker and J., Villasenor, 1992, Decorrelation in interferometric radar echoes. IEEE Transactions on Geoscience and Remote Sensing, 30, 950-959.

[5] R.M. Goldstein and C.L. Werner, 1998, Radar interferogram filtering for geophysical applications. Geophysical Research Letters, 25, 4035-4038.

[6] H. Lee and J.G. Liu, 2000, Topographic phase corrected coherence estimation using multi-pass differential SAR interferometry: differential coherence. IGARSS 2000, 776-778

(a) SAR amplitude image (b) Simulated SAR image from DEM (c) Unflattened raw interferogram

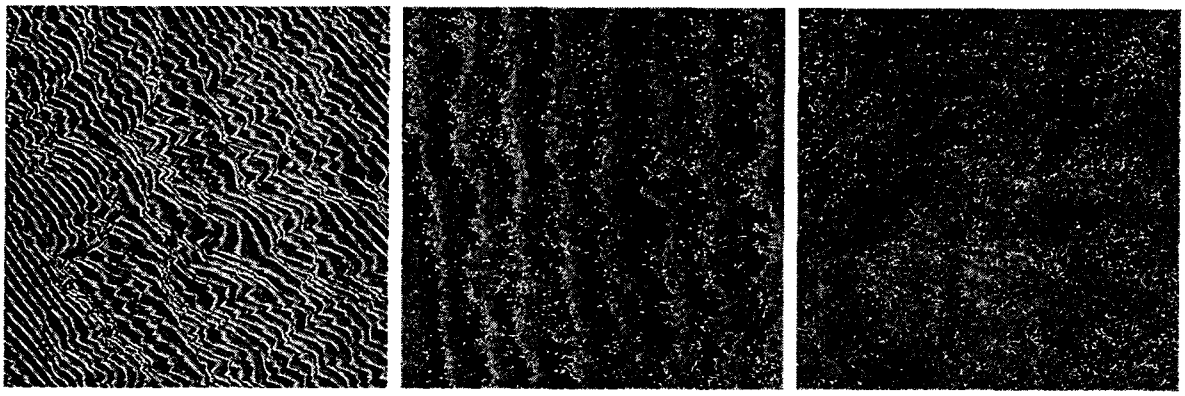

(d) simulated interferogram using initial baseline parameter (e) differential interferogram using initial baseline parameter (f) differential interferogram after baseline refinement

Fig. 2. Processing results